Numerical analysis for the flow past a porous trapezoidal-cylinder based on the stress-jump interfacial-conditions

Received 7 September 2007
Revised 28 December 2007
Accepted 28 January 2008

X.B. Chen, P. Yu and S.H. Winoto
Department of Mechanical Engineering, National University of Singapore, Singapore, and
H.T. Low
Division of Bioengineering, National University of Singapore, Singapore

Abstract

Purpose – The paper aims to report on the flow past a porous trapezoidal-cylinder, in which the porous-fluid interface was treated by implementing the stress jump boundary conditions.

Design/methodology/approach – The numerical method was based on the finite-volume method with body-fitted and multi-block grids. The Brinkman-Forcheimmer extended model was used to govern the flow in the porous medium region. At its interface, a shear stress jump that includes the inertial effect was imposed, together with a continuity of normal stress.

Findings – The present model was validated by comparing with those for the flow around a solid circular cylinder. Results for flow around porous expanded trapezoidal cylinder are presented with flow configurations for different Darcy number, 10^{-2} to 10^{-7}, porosity from 0.4 to 0.8, and Reynolds number 20 to 200. The flow develops from steady to unsteady periodic vortex shedding state. The first coefficient β has a more noticeable effect, whereas the second coefficient β_1 has very small effect, even for $Re = 200$.

Originality/value – The effects of the porosity, Darcy number and Reynolds number on lift and drag coefficients, and the length of circulation zone or shedding period are studied.

Keywords Porous materials, Liquid flow, Laminar flow, Numerical analysis

Paper type Research paper

Nomenclature

A	discretization coefficients using SIMPLEC method
C_D	drag coefficient
C_F	Forchheimer coefficient
C_L	lift coefficient
Da	Darcy number
H	the higher height of the cylinder m
K	permeability of porous medium (m^2)
n	unit vector along normal direction of the interface
p, p^*	local average and intrinsic average pressure (Pa)
P, P^*	dimensionless average and intrinsic average pressure
Re	Reynolds number
t	time (s)
T	dimensionless time
U	dimensionless velocity
U_∞	dimensionless incoming flow velocity
u, v	dimensional velocity (m/s)

International Journal of Numerical Methods for Heat & Fluid Flow
Vol. 19 No. 2, 2009
pp. 223-241

0961-5539
DOI 10.1108/09615530910930982

Greek symbols

β stress jump parameter related to viscous effect

β_1 stress jump parameter related to inertia effect

ε porosity

ε_c convergence error

μ dynamic viscosity (N s/m^2)

ρ fluid density (kg/m^3)

φ general dependent variable

$\Delta\Omega$ finite volume of the control cell

Subscripts

fluid fluid part

i, j grid node number in x and y directions

l east, west, north and south point of control volume

n normal direction to the interface

interface interface value

p control volume center point

porous porous part

t tangential direction to the interface

Superscript

m iteration time step for each time level

1. Introduction

The flow past bluff bodies, especially cylinders, has been investigated extensively for a long time, as they can be applied in the designs of tower structures, suspension bridges, chimneys, heat exchangers, road vehicles, tall buildings, flow meters and other devices. Most of these studies concentrated on the circular cylinder case under free flow conditions as reviewed by Williamson (1996) and Zdravkovich (1997). The flow past square cylinder case has been investigated by Davis and Moore (1982), Davis *et al.* (1984, Franke *et al.* (1990), Klekar and Pantankar (1992), Suzuki *et al.* (1993) and others. They have provided numerical and experimental data about lift coefficient, drag coefficient, base pressure and Strouhal frequency for a range of Reynolds number up to 2,800.

Trapezoidal cylinders are also often used in engineering applications, and the flow around them is more complicate. Lee (1998a, b) numerically studied the early stages of an impulsively started unsteady laminar flow past tapered and expanded trapezoidal cylinders, with *Re* ranging from 25 to 1,000. He showed that the flow starts with no separation first, then the symmetrical circulation zone develops after the rear of the cylinder, later with separated flow and separation bubbles. Finally, the bubbles merge to be a complex flow regime with its own distinct characteristics. Cheng and Liu (2000) simulated the effects of afterbody shape on flow around prismatic cylinders. Their shape of the cross-section of the cylinder varies from square to trapezoidal and finally to triangle one. Later, the laminar vortex shedding from a trapezoidal cylinder with different height ratios was studied by Chung and Kang (2000). They showed that the Strouhal numbers from trapezoidal cylinders with $Re = 100$ and 150, had their minimum values at height ratio of 0.7 and 0.85, respectively, whereas with $Re = 200$, they increases to a maximum value at height ratio of 0.7, then decreases with the increase of height ratio. Kahawita and Wang (2002) also numerically investigated the wake flow behind trapezoidal bodies, using the spline method of fractional steps and they found the trapezoidal height is the dominant influence on Strouhal number, compared with the base width.

However, most of the studies focused on the flow past impermeable bodies, and the flow behind a porous body has not been extensively investigated. Porous bodies may be used to enhance the heat transfer using high-conductivity materials or to damp the flow unsteadiness with low-permeability materials. A related flow is that over a circular cylinder with surface suction and blowing, which was theoretically investigated by Cohen (1991). He derived a model for *St–Re* relationship by order of magnitude estimation. Ling *et al.* (1993) numerically verified this model for flow over a square cylinder and obtained a similar trend between Strouhal and Reynolds numbers. These studies on the effects of suction and blowing through the body may help to explain the behavior of flow past porous bodies.

Jue (2003) simulated vortex shedding behind a porous square cylinder by finite element method. In his study, a general non-Darcy porous media model was applied to describe the flows both inside and outside the cylinder. A harmonic mean was used to treat the sudden change between the fluid and porous medium and no special treatment at the interface was given. He found that Darcy number has more influence on the flow field than porosity does. Bhattacharyya *et al.* (2006) simulated the flow around a porous circular cylinder with Reynolds number ranging from 1 to 40. For the interface, the harmonic-mean formulation was also used to handle the abrupt changes of permeability and porosity. Such abrupt changes were a major source of numerical difficulties and the resultant instabilities in the single-domain approach.

Another method for dealing with the flow in composite domains is the two-domain approach, for example, those of Gartling *et al.* (1996), Costa *et al.* (2004) and Betchen *et al.* (2006), which solves separately the two sets of governing equations in porous and fluid domains. The porous–fluid interface conditions are essential for solving the governing equations in the fluid and porous regions as they are applied at the interface to couple the two sets of equations. The interface condition development has been reviewed in previous papers by Yu *et al.* (2007) and Chen *et al.* (2008a, b, c).

The stress jump condition at the interface was deduced by Ochoa-Tapia and Whitaker (1995a, b) based on the non-local form of the volume averaged method. Based on the Forchheimer equation with the Brinkman correction and the Navier–Stokes equations, Ochoa-Tapia and Whitaker (1998) developed another stress jump condition which includes the inertial effects. Two coefficients appear in this jump condition: one is associated with an excess viscous stress and the other is related to an excess inertial stress.

As compared with the stress-jump boundary-condition which has been rigorously derived, the harmonic mean formulation in the single-domain approach is an artefact to avoid numerical instabilities. Thus, its physical representation of momentum conservation at the interfacial region depends on the relevance of the discretization scheme (Goyeau *et al.* 2003). On the other hand, the main drawback of the stress jump condition is that its parameters are unknown. This closure problem has been investigated by many researchers recently (Goyeau *et al.*, 2003; Chandesris and Jamet, 2006, 2007; Valdes-Parada *et al.*, 2007) and derivations have been proposed to evaluate the first stress-jump parameter which is viscous related.

The implementation of the numerical methodology on the stress jump condition based on Ochoa-Tapia and Whitaker (1995a, b) can be found in the work of Kuznetsov (1997, 1998, 1999), Alazmi and Vafai (2001) and Silva and de Lemos (2003) for parallel flows. In their studies, only the jump in shear stress was included and no special treatment on velocity derivatives was mentioned. However, for flow in general, it is needed to consider how to formulate the velocity derivatives at the interface. Also, for the two-dimensional problem, the normal stress condition is needed to close the sets of equations.

Yu *et al.* (2007) developed a numerical method to treat the interface between a homogeneous fluid and porous medium, based on body-fitted and multi-block technology. At the interface, the shear stress jump including inertia effect, suggested by Ochoa-Tapia and Whitaker (1998), together with the continuity of normal stress is imposed. Later, Chen *et al.* (2008a, b) extended this numerical method to forced convection problems, and the stress jump parameter effects on heat transfer were also considered. Chen *et al.* (2008c) numerically investigated the steady and unsteady flow past a porous square cylinder, implementing the stress jump treatments for the porous–fluid interface. They found that the stress jump interface condition can cause flow instability. The first coefficient β has a more noticeable effect, whereas the second coefficient β_1 has very small effect, even for $Re = 200$.

The objective of the present study was to implement the numerical method developed by Chen *et al.* (2008c) to study the flow around porous trapezoidal cylinder. A two-domain approach is adopted in order to allow for the flexibility of incorporating different types of interface conditions. At the interface, the flow boundary condition imposed is a stress jump, which includes the inertial effect, together with a continuity of normal stress. In the simulation, steady and unsteady flows around a porous expanded trapezoidal cylinder are both considered, with *Re* from 20 to 200, Darcy number from 10^{-2} to 10^{-7}, porosity from 0.4 to 0.8. The effects of stress jump interface condition on the drag coefficient, lift coefficient and shedding period are also studied.

2. Mathematical model

A two-dimensional, laminar and incompressible flow past a porous trapezoidal cylinder is considered here (Figure 1(a)). The fluid is Newtonian and the properties of the fluid are assumed to be constant.

The governing equations for a homogenous fluid region, using vector form, can be written as:

$$\nabla \bullet \vec{u} = 0 \tag{1}$$

$$\rho \frac{\partial u}{\partial t} + \nabla \bullet (\rho \vec{u}\vec{u}) = -\nabla p + \mu \nabla^2 \vec{u} \tag{2}$$

where p is the pressure; ρ is the mass density of the fluid; and μ is the fluid dynamic viscosity.

The porous medium is considered to be rigid, homogeneous and isotropic; and saturated with the same single-phase fluid as that in the homogenous fluid region. Considering viscous and inertial effects, the governing equations for porous region based on Darcy–Brinkman–Forchheimer extended model can be expressed as with Hsu and Cheng (1990) and Nithiarasu *et al.* (2002):

$$\nabla \bullet \vec{u} = 0 \tag{3}$$

$$\underbrace{\rho \frac{\partial \vec{u}}{\partial t}}_{\textit{Unsteady Term}} + \underbrace{\nabla \bullet \left(\frac{\rho \vec{u}\vec{u}}{\varepsilon} \right)}_{\textit{Convective Term}} = -\underbrace{\nabla (\varepsilon p^*)}_{\textit{Pressure Term}} + \underbrace{\mu \nabla^2 \vec{u}}_{\textit{Brinkman Term}} - \underbrace{\frac{\mu \varepsilon}{K} \vec{u}}_{\textit{Darcy Term}} - \underbrace{\frac{\rho \varepsilon C_F |\vec{u}|}{\sqrt{K}} \vec{u}}_{\textit{Forchheimer Term}} \tag{4}$$

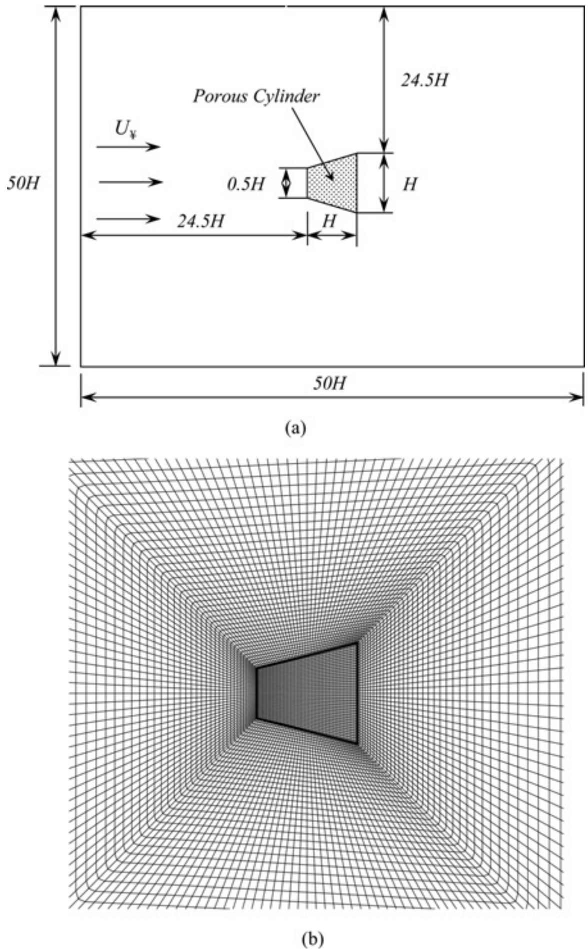

Figure 1.
Schematic of flow past a porous expanded trapezoidal cylinder: (a) computational domain and (b) mesh illustration

where $\vec{u}$ is the local average velocity vector (Darcy velocity); p^* is the intrinsic average pressure; μ is the fluid dynamic viscosity; ε is the porosity; K is the permeability; and C_F is Forchheimer coefficient. Note that throughout the paper, viscosity means dynamic viscosity of the fluid but not the effective (Brinkman) viscosity. The superscript * denotes the intrinsic average. The local average and intrinsic average can be linked by the Dupuit–Forchheimer relationship, for example, $p = \varepsilon p^*$.

At the interface between the homogeneous fluid and porous medium regions, additional boundary conditions must be applied to couple the flows in the two regions. In the present study, the stress jump condition of Ochoa-Tapia and Whitaker (1998) is applied:

$$\frac{\mu}{\varepsilon}\frac{\partial u_t}{\partial n}\bigg|_{porous} - \mu\frac{\partial u_t}{\partial n}\bigg|_{fluid} = \beta\frac{\mu}{\sqrt{K}}u_t\bigg|_{interface} + \beta_1 \rho u_t^2 \tag{5}$$

where in the porous medium region, u_t is the Darcy velocity component parallel to the interface aligned with the direction t and normal to the direction n, whereas in the homogenous fluid region u_t is the fluid velocity component parallel to the interface; β and β_1 are adjustable parameters which account for the stress jump at the interface.

Ochoa-Tapia and Whitaker (1998) derived analytical expressions for parameters β and β_1 which indicate their dependence on permeability and porosity. They concluded that these two parameters are both of order one. Ochoa-Tapia and Whitaker (1995b) experimentally determined that β varies from $+0.7$ to -1.0 for different materials with permeability varying from 9.68×10^{-9} to $8.19\times10^{-8}\mathrm{m}^2$ and average pore size from 4.06×10^{-4} to $1.14\times10^{-3}\mathrm{m}$.

There have been analytical studies which tried to relate the stress jump parameter β to the properties of the porous media. Min and Kim (2005) considered channel flow which has a partial porous-medium with periodic structure (solid and fluid phases repeating in a regular pattern). For the fluid layer, the periodic velocity distribution at the interface was expressed as a cosine Fourier series. The control equations for the fluid and porous regions were solved analytically to obtain the shear stress differences at the interface. The values of porosity and pore size were those used in Beavers and Joseph (1967). They found that the stress jump parameter β was of order one and depended on local porosity, Darcy number, pore diameter and thickness of the adjacent fluid layer. Valdes-Parada *et al.* (2007) proposed a mixed stress tensor to relate the stress jump coefficient β, which was the sum of the global and Brinkman stress contributions. The porous medium was assumed to be composed of equally spaced spheres or cylinders. Their predicted values of the stress jump coefficient β ranged from 0.96 to 1.25, for pore sizes and porosities used in Beavers and Joseph (1967). From the above two studies, it is noted that the stress jump coefficient β was found to be of order one for two very different types of porous structures.

There is presently no experimental or numerical data for the second stress jump parameter β_1. Ochoa-Tapia and Whitaker (1998) theoretically derived its expression and expected its values to be of order one. It is not known how much the two parameters may change from one type of interface to another; and it is assumed in this study that the changes should be in the same range as those for different types of materials. Thus, for the purpose of demonstrating the implementation of the present formulation and assessing the sensitivity of the stress jump parameters, both β and β_1 are varied in the range -1.0-$+1.0$ in the present study.

In addition to equation (5), the continuity of velocity and normal stress prevailing at the interface is given by:

$$\vec{u}|_{\mathrm{fluid}} = \vec{u}|_{\mathrm{porous}} = \vec{v}_{\mathrm{interface}} \tag{6}$$

$$\frac{\mu}{\varepsilon}\frac{\partial u_n}{\partial n}\bigg|_{\mathrm{porous}} - \mu\frac{\partial u_n}{\partial n}\bigg|_{\mathrm{fluid}} = 0 \tag{7}$$

where in the porous medium region, u_n is the Darcy velocity component normal to the interface; and in the homogenous fluid region, u_n is the fluid velocity component normal to the interface. By combining with the appropriate boundary conditions of the composite region, equations (1) to (7) can be used to simulate the flow in a system composed of a porous medium and a homogenous fluid.

The equations (1) to (4) can be non-dimensionalized as following (Chen *et al.*, 2008a):

For fluid domains,

$$\nabla \bullet \vec{U} = 0 \tag{8}$$

$$\frac{\partial \vec{U}}{\partial T} + \nabla \bullet \left(\vec{U}\vec{U} \right) = -\nabla P + \frac{1}{Re} \nabla^2 \vec{U} \tag{9}$$

For porous domains,

$$\nabla \bullet \vec{U} = 0 \tag{10}$$

$$\frac{\partial \vec{U}}{\partial T} + \nabla \bullet \left(\frac{\vec{U}\vec{U}}{\varepsilon} \right) = -\nabla(\varepsilon P^*) + \frac{1}{Re} \nabla^2 \vec{U} - \frac{\varepsilon}{Da \bullet Re} \vec{U} - \frac{\varepsilon C_F \left| \vec{U} \right|}{\sqrt{Da}} \vec{U} \tag{11}$$

with the following dimensionless interface conditions,

$$\frac{1}{\varepsilon} \frac{\partial U_t}{\partial n} \bigg|_{\text{porous}} - \frac{\partial U_t}{\partial n} \bigg|_{\text{fluid}} = \beta \frac{1}{\sqrt{Da}} U_t \bigg|_{\text{interface}} + \beta_1 \bullet Re \bullet U_t^2 \tag{12}$$

$$\vec{U} \bigg|_{\text{fluid}} = \vec{U} \bigg|_{\text{porous}} = \vec{U}_{\text{interface}} \tag{13}$$

$$\frac{1}{\varepsilon} \frac{\partial U_n}{\partial n} \bigg|_{\text{porous}} - \frac{\partial U_n}{\partial n} \bigg|_{\text{fluid}} = 0 \tag{14}$$

where Re is Reynolds number, $Re = \rho U_\infty H / \mu$ and Da is Darcy number, $Da = K/H^2$.

3. Numerical method

In the present study, the SIMPLEC method developed by van Doormal and Raithby (1984), is applied to couple the velocity and pressure. The second-order central difference scheme was applied to discretize the governing equations. All the steady-state terms in the equations are discretized using the implicit scheme. For the unsteady source term, a three-level second-order scheme is used. The details for the governing equation discretizaiton and interface treatment can be found in Yu *et al.* (2007) and Chen *et al.* (2008c).

To avoid oscillations in the pressure or velocity, the interpolation proposed by Rhie and Chow (1983) is adopted:

$$u_e^m = \overline{(u^m)_e} - \Delta\Omega_e \overline{\left(\frac{1}{A_P^u + \sum_l A_l^u} \right)_e} \left[\left(\frac{\delta p}{\delta x} \right)_e - \overline{\left(\frac{\delta p}{\delta x} \right)_e} \right]^{m-1} \tag{15}$$

where m is iteration step for each time level.

To close the algebra equation system, the pressure at the interface must be determined. However, Betchen *et al.* (2006) pointed out that the pressure gradient at the interface may not be continuous due to the rather large Darcy and Forchheimer terms (equation (4)), which may result in a rapid pressure drop at the porous side. This discontinuity of the pressure gradient becomes more severe at higher Reynolds number and lower Darcy number. Thus, it requires special treatment to estimate the interface pressure from that of the vicinity at either side. A simplistic pressure estimation may give unrealistic, oscillatory velocity profile. The coupling issue of pressure–velocity at the interface was described in a recent paper by Betchen *et al.* (2006) who proposed a solution that enables stable calculations. The pressure is extrapolated in the fluid side to a location at a small distance near the interface. From this location, a momentum balance is then used to estimate the interface pressure. This estimate is then averaged with the pressure extrapolated from the porous side to obtain the interface pressure. In the present paper, a less complex treatment was adopted. Extrapolations from the fluid and porous sides give two different estimates of the interface pressure. The average of the two estimates is used as the interface pressure. A small number of iterations is required for accuracy.

4. Results and discussion

In the following computations, Forchheimer coefficient is set $C_F = 1.75/\sqrt{(150\varepsilon^3)}$, as used by Nithiarasu *et al.* (1999). Non-uniform, body-fitted and non-orthogonal meshes are employed, where the density of meshes around the cylinder is larger than those areas far away (Figure 1(b)). At the left boundary, the incoming flow is uniform, and at the other three boundaries, $U/n = 0$. The initial conditions for the computation were either uniform flow at the inlet $U_\infty = 1.0$, or the results of a previous calculation, often at different Reynolds number, Darcy number or porosity values. The time step is set equal to 10^{-2}, and the convergence criteria for each time level is set as follows,

$$\sum \left| \varphi_{i,j}^{m+1} - \varphi_{i,j}^{m} \right| / \sum \varphi_{i,j}^{m+1} \leq \varepsilon_c \tag{16}$$

where $\varepsilon_c = 10^{-6}$.

To validate the present program, the drag and lift coefficients for the flow around a circular cylinder are compared with those in previous studies. The results shown in Table I agree well with the benchmark studies. A grid independency survey was conducted for $Re = 200$, $\varepsilon = 0.4$, $Da = 10^{-4}$ and $\beta = 0$, $\beta_1 = 0$. It shows that when the

Table I.
Comparison of drag and lift coefficients with previous studies

	$Re = 100$		$Re = 200$	
	C_D	C_L	C_D	C_L
Braza *et al.* (1986)	1.36 ± 0.015	± 0.250	1.40 ± 0.050	± 0.75
Liu *et al.* (1998)	1.35 ± 0.012	± 0.339	1.31 ± 0.049	± 0.69
Calhoun (2002)	1.33 ± 0.014	± 0.298	1.17 ± 0.058	± 0.67
Present	1.38 ± 0.009	± 0.335	1.36 ± 0.050	± 0.73

grid number in the porous domain was kept at 62×62 constant, increasing the grid number in the fluid domain outside from 320×140 to 360×160 resulted in 3 per cent change for shedding period, lift and drag coefficients. Further increasing the grid number larger than 360×160 did not change them >1 per cent. Thus, considering the

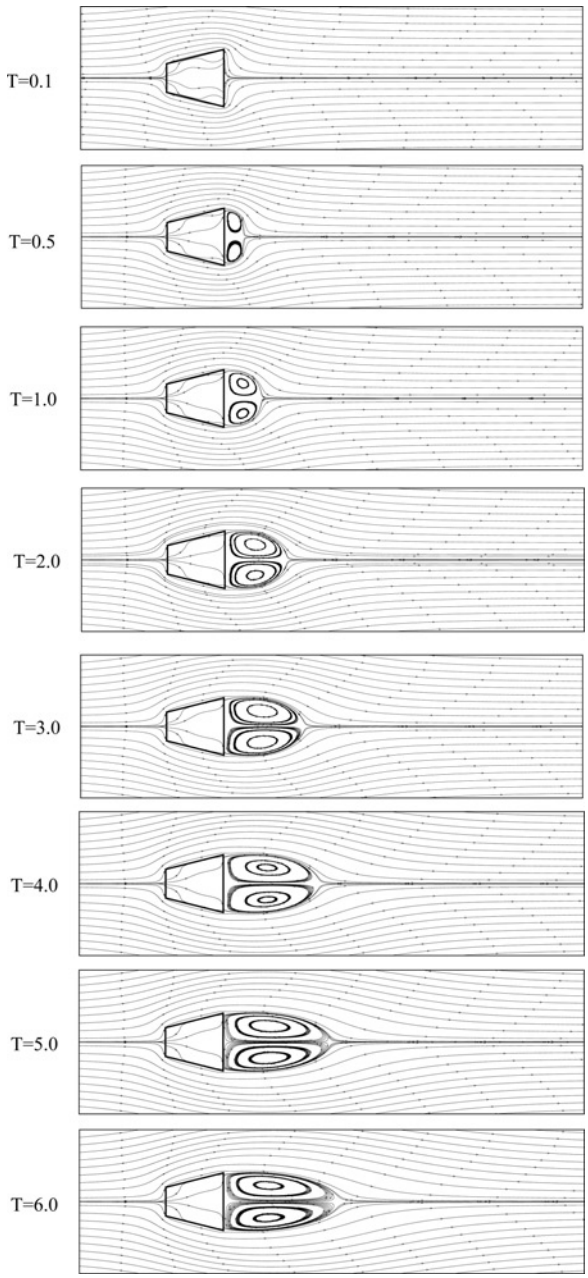

Figure 2.
Instantaneous streamline pattern for $Re = 40$ at various times, with $\varepsilon = 0.4$, $Da = 10^{-4}$ and $\beta = 0$, $\beta_1 = 0$

computational cost and accuracy, a 360×160 mesh for the fluid domain with 62×62 mesh for the porous domain is enough for use in subsequent computations.

Figure 2 shows the early stage development of streamline patterns for $Re = 40$, $\varepsilon = 0.4$, $Da = 10^{-4}$ and $\beta = 0$, $\beta_1 = 0$. There is no visible separation flow downstream of

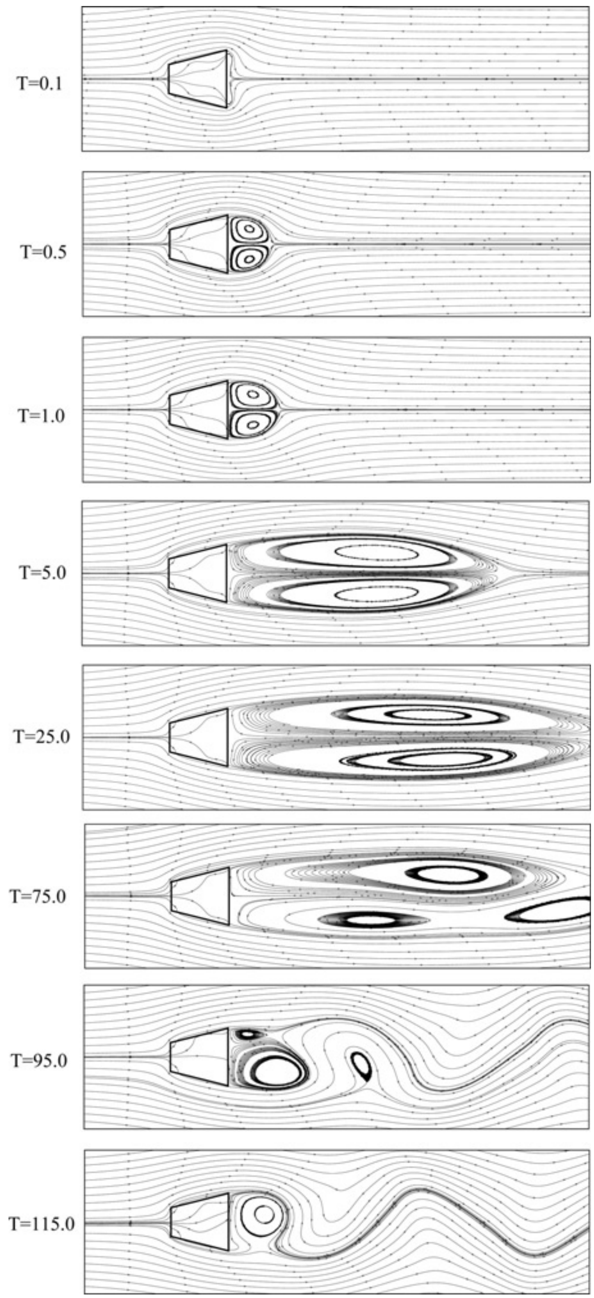

Figure 3.
Instantaneous streamline pattern for $Re = 200$ at various times, with $\varepsilon = 0.4$, $Da = 10^{-4}$ and $\beta = 0$, $\beta_1 = 0$

the cylinder for $t \leq 0.1$. After a short lapse of time, the flow separates from the rear surface of the cylinder forming a recirculation zone which has two symmetrical eddies. After a certain lapse of time, the size of these two eddies become larger and finally they reach a constant shape at steady-state flow ($T = 6.0$).

Figure 3 shows the flow development history at a higher $Re = 200$. Compared with the previous $Re = 40$, the flow also starts with no separation. However, subsequently the twin eddies after the cylinder develop faster and bigger. When $T = 75.0$, one eddy breaks into two and tends to separate from the cylinder far away. Vortex shedding phenomena happens at $t = 95.0$, and finally, the flow has a periodic pattern ($T = 115.0$). Figure 4 shows the drag and lift coefficient history developments. The results show that the vortex shedding becomes periodic, and the frequency of the lift coefficient is twice that of the drag coefficient, which are consistent with those of solid ones (Davis and Moore, 1982).

Figure 5 shows the instantaneous streamlines for different Reynolds number, at dimensionless time $T = 150.0$, constant porosity $\varepsilon = 0.4$, Darcy number $Da = 10^{-4}$, jump coefficients $\beta = 0$ and $\beta_1 = 0$. The flow phenomenon of this case is like those of the non-porous one. At $Re = 20$, a closed steady recirculation region consisting of twin symmetric vortices forms behind the cylinder. This recirculation region increases in size with the increase in Reynolds number, as shown for $Re = 40$. When the Reynolds number becomes larger, the flow becomes unsteady; the vortices in the separation bubble start to separate alternatively from the trailing edge of the square cylinder and move downstream, which is the vortex shedding phenomena.

Figure 6 shows the variation of recirculation length with Darcy number. As shown, the recirculation length becomes longer when Darcy number is lower, because there is less porous flow through the cylinder. At very low Darcy number, there is very little porous flow and thus the recirculation length approaches to an asymptotic value near to that of a solid one. At $Da = 10^{-2}$, there is no recirculation length as there is no vortex formation behind the cylinder.

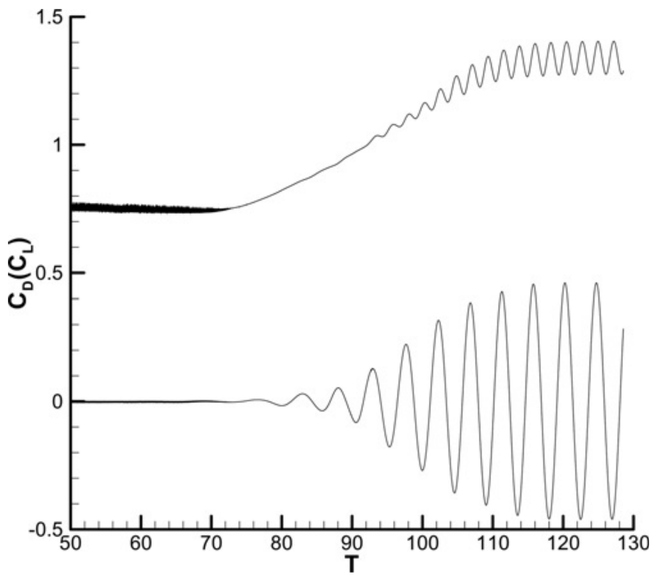

Figure 4.
Drag (up) and lift (down) coefficient histories, at $Re = 200$, $\varepsilon = 0.4$, $Da = 10^{-4}$ and $\beta = 0$, $\beta_1 = 0$

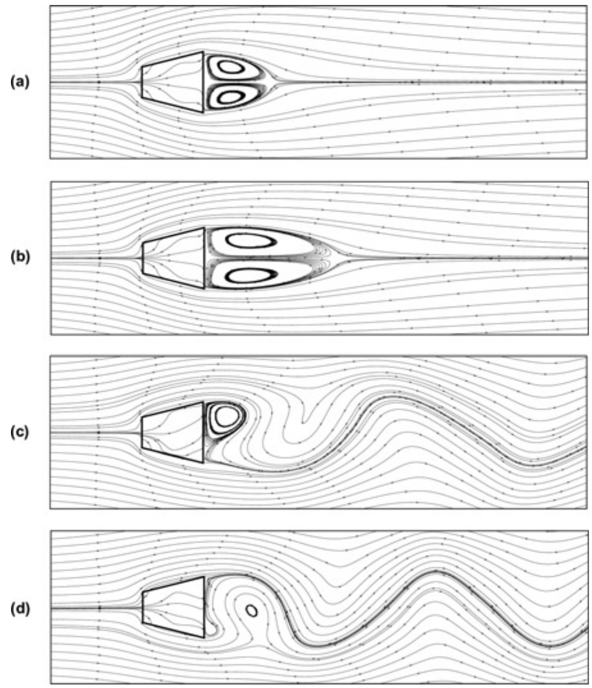

Figure 5.
Instantaneous streamline contours at $T = 150.0$, $\varepsilon = 0.4$, $Da = 10^{-4}$, and $\beta = 0$, $\beta_1 = 0$: (a) $Re = 20$, (b) $Re = 40$, (c) $Re = 100$ and (d) $Re = 200$

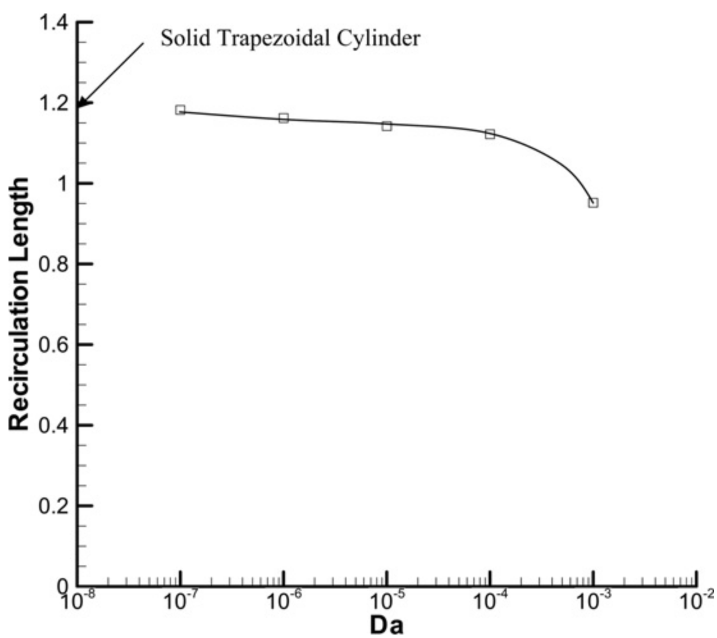

Figure 6.
Variation of recirculation length with Darcy number at $\varepsilon = 0.4$, $Re = 20$ and $\beta = 0$, $\beta_1 = 0$

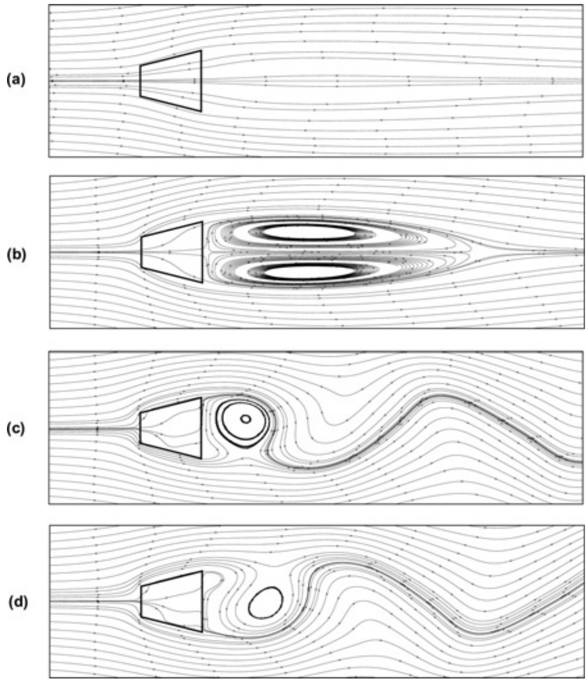

Figure 7.
Instantaneous streamline contours at $T = 120$, $\varepsilon = 0.4$, $Re = 100$ and $\beta = 0$, $\beta_1 = 0$: (a) $Da = 10^{-2}$, (b) $Da = 10^{-3}$, (c) $Da = 10^{-4}$ and (d) $Da = 10^{-5}$

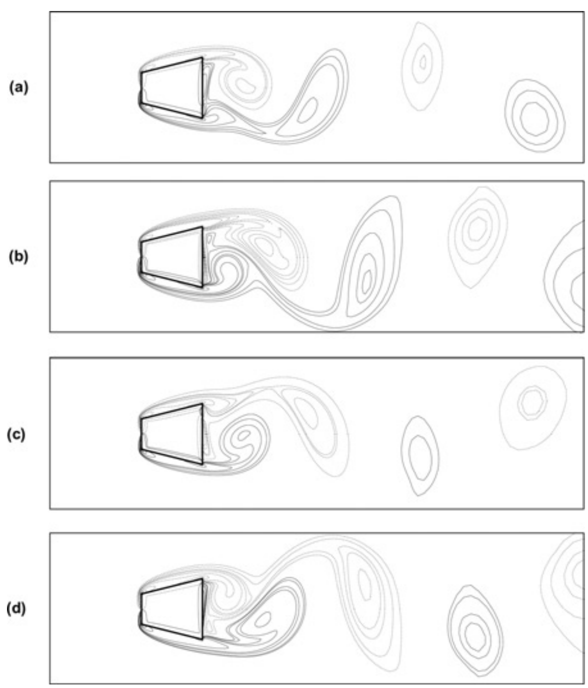

Figure 8.
Vorticity contours in a period $\tau_p = 4.42$ from $T = 125.0$ at $Re = 200$, $\varepsilon = 0.4$, $Da = 10^{-4}$ and $\beta = 0$, $\beta_1 = 0$: (a) $C_L = C_{L\min} = -0.460$, from positive to negative, (b) $C_L = \min$, (c) $C_L = 0$, from negative to positive and (d) $C_L = C_{L\max} = +0.460$

Figure 7 shows the instantaneous streamline contours for different Darcy number at higher $Re = 100$. It can be seen that when $Da = 10^{-2}$, there is no vortex formation behind the cylinder. And when $Da = 10^{-3}$, the flow show steady characteristic with two vortices after the cylinder. When Da decreases from 10^{-4} to 10^{-5}, with less porous flow through the cylinder, the flow pattern becomes unsteady, and the vortex begins to separate. Figure 8 shows this vortex contour in one period. It is shown that, different from the solid one, the vortex formulation extends to the porous part. The two main vortex after the cylinder interact with each other to generate negative or positive lift forces. However, at $Re = 250$, for the drag coefficient shown in Figure 9, it is not a simple sine wave and there seems to be a small modulation in shedding frequency. This kind of phenomena was also found for the solid case by Davis and Moore (1982). In the following study, the Re ranges from 20 to 200.

Table II shows the influence of the stress jump parameters β and β_1 at the lower Reynolds numbers $Re = 20$ and 40, with $\varepsilon = 0.4$ and $Da = 10^{-4}$. The β effect is noticeable, especially for negative values, whereas β_1 has less effect. From equation (5),

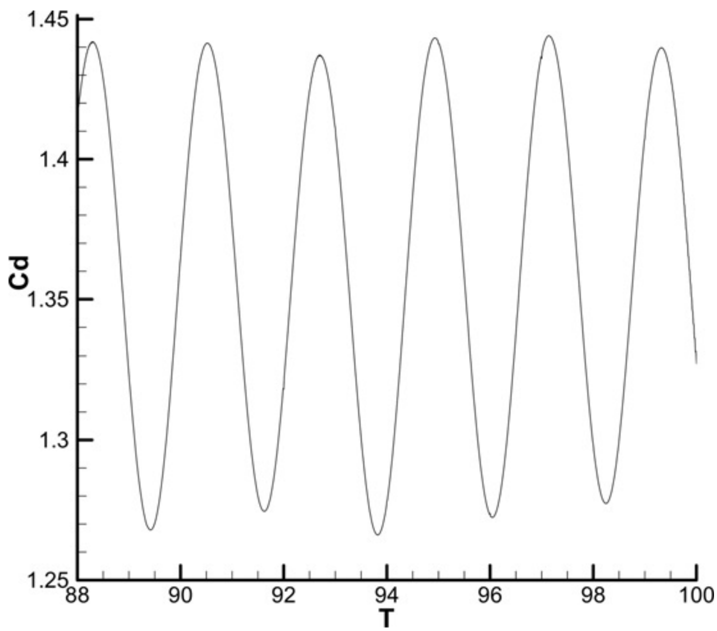

Figure 9.
Periodic drag coefficient histories, at $Re = 250$, $\varepsilon = 0.4$, $Da = 10^{-4}$ and $\beta = +1.0$, $\beta_1 = 0$

Table II.
Drag coefficient and length of the recirculation zone, for low Re, with $\varepsilon = 0.4$ and $Da = 10^{-4}$

Re	β	β_1	C_D	L/H	Re	β	β_1	C_D	L/H
20	−1.0	0	1.602	1.06	40	−1.0	0	1.192	2.01
	0	0	1.826	1.12		0	0	1.345	2.13
	1.0	0	1.877	1.14		1.0	0	1.375	2.14
	0	−1.0	1.816	1.12		0	−1.0	1.342	2.13
	0	0	1.826	1.12		0	0	1.345	2.13
	0	1.0	1.826	1.12		0	1.0	1.346	2.13

if the permeability K is small, that is Darcy number is small, the viscous term $\beta\left(\frac{\mu}{\sqrt{K}}\right)u_t$ is large. It is noted in Table II that the recirculation lengths are not much affected by the stress jump parameters. That is, these parameters do not affect the flow patterns at these lower Reynolds numbers of 20 and 40. This observation is different from a previous study (Chen *et al.*, 2008c) on porous square cylinders where the parameters tend to make the flow more unstable.

Table III shows the influence of the stress jump parameters β and β_1 on the vortex shedding period τ_p, lift and drag coefficients C_L, C_D at the higher Reynolds numbers $Re = 100$ and 200, with $\varepsilon = 0.4$ and $Da = 10^{-4}$. It can be seen that for the same Reynolds number, β effect is still more obvious than β_1. Yu *et al.* (2007) showed that the viscous term $\beta\left(\frac{\mu}{\sqrt{k}}\right)u_t$ effect dominates for $Re = 20$, and suggested that the inertial term $\beta_1 \rho u_t^2$, in equation (5), may be important at high Reynolds number. However, the Reynolds number in the present study was not increased above 200 to avoid the complications from three-dimensional flow and the frequency modulation noted above. It can be seen that when β

Re	β	β_1	τ_p	C_L	C_D (amplitude)
100	0	1.0	5.47	−0.207-0.207	1.199-1.224 (0.025)
	0	0	5.41	−0.206-0.206	1.199-1.225 (0.026)
	0	−1.0	5.48	−0.207-0.207	1.198-1.225 (0.027)
	1.0	0	5.51	−0.211-0.211	1.222-1.249 (0.027)
	0	0	5.41	−0.206-0.206	1.199-1.225 (0.026)
	−1.0	0	5.37	−0.192-0.192	1.099-1.122 (0.023)
200	0	1.0	4.50	−0.451-0.451	1.258-1.395 (0.137)
	0	0	4.42	−0.460-0.460	1.275-1.405 (0.130)
	0	−1.0	4.63	−0.487-0.487	1.284-1.431 (0.147)
	1.0	0	4.53	−0.472-0.472	1.296-1.432 (0.136)
	0	0	4.42	−0.460-0.460	1.275-1.405 (0.130)

Table III. Drag, lift and shedding period for high Re with unsteady vortex shedding, with $\varepsilon = 0.4$ and $Da = 10^{-4}$

Re	Da	τ_p	C_L	C_D (amplitude)	L/H
20	10^{-5}	–	0	1.838	1.14
	10^{-4}	–	0	1.826	1.12
	10^{-3}	–	0	1.805	0.95
	10^{-2}	–	0	1.610	–
40	10^{-5}	–	0	1.353	2.22
	10^{-4}	–	0	1.345	2.13
	10^{-3}	–	0	1.330	1.94
	10^{-2}	–	0	1.210	–
100	10^{-5}	5.46	−0.235-0.235	1.294-1.329 (0.035)	–
	10^{-4}	5.41	−0.206-0.206	1.199-1.225 (0.026)	–
	10^{-3}	5.52	−0.116-0.116	1.164-1.171 (0.007)	–
	10^{-2}	–	0	0.895	–
200	10^{-5}	4.58	−0.552-0.552	1.356-1.570 (0.214)	–
	10^{-4}	4.42	−0.460-0.460	1.275-1.405 (0.130)	–
	10^{-3}	4.62	−0.175-0.175	1.125-1.147 (0.022)	–
	10^{-2}	–	0	0.772	–

Table IV. Effect of Darcy number with $\varepsilon = 0.4$, $\beta = 0$ and $\beta_1 = 0$

Table V.
Effect of porosity with $Da = 10^{-4}$ and $\beta = 0$, $\beta_1 = 0$

Re	ε	τ_p	C_L	C_D (amplitude)	*L/H*
20	0.4	–	0	1.826	1.12
	0.6	–	0	1.768	1.12
	0.8	–	0	1.713	1.11
40	0.4	–	0	1.345	2.13
	0.6	–	0	1.314	2.12
	0.8	–	0	1.281	2.12
100	0.4	5.41	−0.206-0.206	1.199-1.225 (0.026)	–
	0.6	5.47	−0.207-0.207	1.178-1.205 (0.027)	–
	0.8	5.53	−0.208-0.208	1.158-1.184 (0.026)	–
200	0.4	4.42	−0.460-0.460	1.275-1.405 (0.130)	–
	0.6	4.46	−0.462-0.462	1.257-1.389 (0.132)	–
	0.8	4.49	−0.464-0.464	1.243-1.377 (0.134)	–

increases from -1.0 to $+1.0$, the average drag coefficient, and the amplitude of both lift and drag coefficients, and the shedding period show increasing trends. When β_1 increases from -1.0 to $+1.0$, the change is not large. This shows that in equation (5), the viscous term $\beta\left(\frac{\mu}{\sqrt{k}}\right)u_t$ is more important than the inertial term $\beta_1 \rho u_t^2$.

Table IV shows the influence of Darcy number. For the steady cases, $Re = 20$ and 40, the drag coefficient and length of recirculation zone decreases when the Darcy number increases. This is due to more porous flow. It can be seen that the results for $Da = 10^{-4}$ and 10^{-5} changes little, as for $Da \leq 10^{-4}$, the flow inside the porous media is rather small, called Darcy flow conventionally. For $Re = 100$ and $Re = 200$, it is interesting to find that the flow is still steady when $Da = 10^{-2}$. For the unsteady cases, $Re = 100$ and 200, while Da decreases from 10^{-3} to 10^{-5}, the average drag coefficient, and the amplitude of both lift and drag coefficients, show increasing trends, whereas for the shedding period, there is no obvious trend. The flow is more complicated because the porous flow may affect the location of the streamline separation near the back edge of the cylinder (instantaneous streamlines in Figure 7).

Table V shows that at higher porosity, there is decrease of drag coefficient (average for unsteady cases). For the unsteady cases, the lift amplitude is larger at higher porosity. This behavior may be explained by the effect of more porous flow through the cylinder. There are not much effect of porosity on recirculation length and shedding period. However, the effect of porosity is smaller than that of Darcy number, which is consistent with the porous square case found by Jue (2003) and Chen *et al.* (2008c).

5. Conclusion

The two-dimensional flow around a porous expanded trapezoidal cylinder has been carried out numerically using finite-volume method, based on the body-fitted, non-orthogonal grids and multi-block technology. The flow in porous region is described by the generalized Darcy–Brinkman–Forchheimer extended model, which considers the inertia, convective and viscous effects. To couple the flows at the interface, the shear-stress jump condition is implemented.

The flow range considered was varied from steady state to unsteady Reynolds number 200 and different porosities, Darcy numbers and stress jump parameters were considered. With a larger Darcy number, the Reynolds number has to be higher before the vortex shedding phenomena occurs. The effects of the stress jump parameters, β

and β_1 ranging from -1.0 to $+1.0$, are given for the flow condition from $Re = 20$ to 200. The first coefficient β has a more noticeable effect, whereas the second coefficient β_1 has small effect, even for $Re = 200$. The Darcy number effect becomes smaller when $Da \leq 10^{-4}$; at larger Darcy number, the fluctuation-amplitude of drag coefficient decreases. Generally, a larger porosity cylinder results in a smaller drag coefficient and larger lift amplitude.

References

Alazmi, B. and Vafai, K. (2001), "Analysis of fluid flow and heat transfer interfacial conditions between a porous medium and a fluid layer", *International Journal of Heat and Mass Transfer*, Vol. 44, pp. 1735-49.

Beavers, G.S. and Joseph, D.D. (1967), "Boundary condition at a naturally permeable wall", *Journal of Fluid Mechanics*, Vol. 30, pp. 197-207.

Betchen, L., Straatman, A.G. and Thompson, B.E. (2006), "A nonequilibrium finite-volume model for conjugate fluid/porous/solid domains", *Numerical Heat Transfer A*, Vol. 49, pp. 543-65.

Bhattacharyya, S., Dhinakaran, S. and Khalili, A. (2006), "Fluid motion around and through a porous cylinder", *Chemical Engineering Science*, Vol. 61, pp. 4451-61.

Braza, M., Chassaing, P. and Minh, H.H. (1986), "Numerical study and physical analysis of the pressure and velocity fields in the near wake of a circular cylinder". *Journal of Fluid Mechanics*, Vol. 165, pp. 79-130.

Calhoun, D. (2002), "A cartesian grid method for solving the two-dimensional streamfunction-vorticity equations in irregular regions", *Journal of Computational Physics*, Vol. 176, pp. 231-75.

Chandesris, M. and Jamet, D. (2006), "Boundary conditions at a planar fluid-porous interface for a Poiseuille flow", *International Journal of Heat and Mass Transfer*, Vol. 49, pp. 2137-50.

Chandesris, M. and Jamet, D. (2007), "Boundary conditions at a fluid-porous interface: An a priori estimation of the stress jump coefficients", *International Journal of Heat and Mass Transfer*, Vol. 50, pp. 3422-36.

Chen, X.B., Yu, P., Winoto, S.H. and Low, H.T. (2008a), "A numerical method for forced convection in porous and homogenous fluid domains coupled at interface by stress jump", *International Journal of Numerical Methods for Fluids*, Vol. 56, pp. 1705–29.

Chen, X.B., Yu, P., Winoto, S.H. and Low, H.T. (2008b), "Forced convection over a backward facing step with a porous floor segment", *Numerical Heat Transfer A*, Vol. 53, pp. 1211–30.

Chen, X.B., Yu, P., Winoto, S.H. and Low, H.T. (2008c), "Numerical analysis for the flow past a porous square cylinder based on the stress-jump interfacial-conditions", *International Journal of Numericla Methods for Heat and Fluid Flow*, Vol. 18 No. 5, pp. 635–55.

Cheng, M. and Liu, G.R. (2000), "Effects of afterbody shape on flow around prismatic cylinders", *Journal of Wind Engineering and Industrial Aerodynamics*, Vol. 84, pp. 181-96.

Chung, Y.J. and Kang, S.-H (2000), "Laminar vortex shedding from a trapezoidal cylinder with different height ratios", *Physics of Fluids*, Vol. 12 No. 5, pp. 1251-4.

Cohen, R.D. (1991), "Predicting the effects of surface suction and blowing on the Strouhal frequencies in vortex shedding", *JSME International Journal (Series II)*, Vol. 34, pp. 30-9.

Costa, V.A.F., Oliveira, L.A., Baliga, B.R. and Sousa, A.C.M. (2004), "Simulation of coupled flows in adjacent porous and open domains using a control-volume finite-element method", *Numerical Heat Transfer A*, Vol. 45, pp. 675-97.

Davis, R.W. and Moore, E.F. (1982), "A numerical study of vortex shedding from rectangles", *Journal of Fluid Mechanics*, Vol. 116, pp. 475-506.

Davis, R.W., Moore, E.F. and Purtell, L.P. (1984), "A numerical-experimental study of confined flow around rectangular cylinders", *Physics of Fluids*, Vol. 27 No. 1, pp. 46-59.

Franke, R., Rodi, W. and Schonung, B. (1990), "Numerical calculation of laminar vortex shedding past cylinders", *Journal of Wind Engineering and Industrial Aerodynamics*, Vol. 35, pp. 237-57.

Gartling, D.K., Hickox, C.E. and Givler, R.C. (1996), "Simulation of coupled viscous and porous flow problems", *Computational Fluid Dynamics*, Vol. 7, pp. 23-48.

Goyeau, B., Lhuillier, D., Gobin, D. and Velarde, M.G. (2003), "Momentum transport at a fluid-porous interface", *International Journal of Heat and Mass Transfer*, Vol. 46, pp. 4071-81.

Hsu, C.T. and Cheng, P. (1990), "Thermal dispersion in a porous medium", *International Journal of Heat and Mass Transfer*, Vol. 33, pp. 1587-97.

Jue, T.C. (2003), "Numerical analysis of vortex shedding behind a porous cylinder", *International Journal of Numerical Methods for Heat Fluid Flow*, Vol. 14, pp. 649-63.

Kahawita, R. and Wang, P. (2002), "Numerical simulation of the wake flow behind trapezoidal bluff bodies", *Computers and Fluids*, Vol. 31, pp. 99-112.

Klekar, K.M. and Patankar, S.V. (1992), "Numerical predication of vortex shedding behind square cylinders", *International Journal of Numerical Methods for Fluid*, Vol. 14, pp. 327-41.

Kuznetsov, A.V. (1997), "Influence of the stress jump condition at the porous medium/clear-fluid interface on a flow at a porous wall", *International Communications in Heat and Mass Transfer*, Vol. 24, pp. 401-10.

Kuznetsov, A.V. (1998), "Analytical investigation of coquette flow in a composite channel partially filled with a porous medium and partially with a clear fluid", *International Journal of Heat and Mass Transfer*, Vol. 41, pp. 2556-60.

Kuznetsov, A.V. (1999), "Fluid mechanics and heat transfer in the interface region between a porous medium and a fluid layer: a boundary layer solution", *Journal of Porous Media*, Vol. 2, pp. 309-21.

Lee, T.S. (1998a), "Early stages of an impulsively started unsteady laminar flow past tapered trapezoidal cylinders", *International Journal Numerical Methods for Fluids*, Vol. 26, pp. 1181–203.

Lee, T.S. (1998b), "Numerical study of early stages of an impulsively started unsteady laminar flow past expanded trapezoidal cylinders", *International Journal of Numerical Methods for Heat and Fluid Flow*, Vol. 8, pp. 934-55.

Ling, L.M., Ramaswamy, B. Cohen, D.R. and Jue, T.C. (1993), "Numerical analysis on Strouhal frequencies in vortex shedding over square cylinders with surface suction and blowing", *International Journal of Numerical Methods for Heat and Fluid Flow*, Vol. 3, pp. 458-67.

Liu, C., Sheng, X. and Sung, C.H. (1998), "Preconditioned multigrid methods for unsteady incompressible flows", *Journal of Computational Physics*, Vol. 139, pp. 35-57.

Min, J.Y. and Kim, S.K. (2005), "A novel methodology for thermal analysis of a composite system consisting of a porous medium and an adjacent fluid layer", *Journal of Heat Transfer*, Vol. 127, pp. 648-56.

Nithiarasu, P., Seetharamu, K.N. and Sundararajan, T. (2002), "Finite element modelling of flow, heat and mass transfer in fluid saturated porous media", *Archives of Computational Methods in Engineering*, Vol. 9, pp. 3-42.

Nithiarasu, P., Sujatha, K.S., Sundararajan, T. and Seetharamu, K.N. (1999), "Buoyancy driven flow in a non-Darcian, fluid-saturated porous enclosure subjected to uniform heat flux – a numerical study", *Communications in Numerical Methods in Engineering*, Vol. 15, pp. 765-76.

Ochoa-Tapia, J.A. and Whitaker, S. (1995a), "Momentum transfer at the boundary between a porous medium and a homogeneous fluid I: theoretical development", *International Journal of Heat and Mass Transfer*, Vol. 38, pp. 2635-46.

Ochoa-Tapia, J.A. and Whitaker, S. (1995b), "Momentum transfer at the boundary between a porous medium and a homogeneous fluid II: comparison with experiment", *International Journal of Heat and Mass Transfer*, Vol. 38, pp. 2647-55.

Ochoa-Tapia, J.A. and Whitaker, S. (1998), "Momentum jump condition at the boundary between a porous medium and a homogeneous fluid: inertial effect", *Journal of Porous Media*, Vol. 1, pp. 201-17.

Rhie, C.M. and Chow, W.L. (1983), "Numerical study of the turbulent flow past an airfoil with trailing edge separation", *AAIA Journal*, Vol. 21, pp. 1525-32.

Silva, R.A. and de Lemos, M.J.S. (2003), "Numerical analysis of the stress jump interface condition for laminar flow over a porous layer", *Numerical Heat Transfer A*, Vol. 43, pp. 603-17.

Suzuki, H., Inoue, Y., Nishimura, T., Fukutani, F. and Suzuki, K. (1993), "Unsteady flow in a channel obstructed by a square rod (crisscross motion of vortex)", *International Journal of Heat and Fluid Flow*, Vol. 14 No. 1, pp. 2-9.

Valdes-Parada, F.J., Goyeau, B. and Ochoa-Tapia, J.A. (2007), "Jump momentum boundary condition at a fluid-porous dividing surface: derivation of the closure problem", *Chemical Engineering Science*, Vol. 62, pp. 4025-39.

van Doormal, J.P. and Raithby, G.D. (1984), "Enhancements of the SIMPLE method for predicting incompressible fluid flows", *Numerical Heat Transfer*, Vol. 7, pp. 147-63.

Williamson, C.H.K. (1996), "Vortex dynamics in the cylinder wake", *Annual Review of Fluid Mechanics*, Vol. 28, pp. 477-539.

Yu, P., Lee, T.S., Zeng, Y. and Low, H.T. (2007), "A Numerical method for flows in porous and homogenous fluid domains coupled at the interface by stress jump", *International Journal of Numerical Methods for Fluids*, Vol. 53, pp. 1755-75.

Zdravkovich, M.M. (1997), *Flow Around Circular Cylinders, Vol. 1: Fundamentals*, Oxford University Press, New York, NY.

Corresponding author
H.T. Low can be contacted at: mpelowht@nus.edu.sg